Observation of Depression Solitary Surface Waves on a Thin Fluid Layer

Éric Falcon,[1,*] Claude Laroche,[1] and Stéphan Fauve[2]

[1]*Laboratoire de Physique, École Normale Supérieure de Lyon, UMR 5672, 46, allée d'Italie, 69 007 Lyon, France*
[2]*Laboratoire de Physique Statistique, École Normale Supérieure, UMR 8550, 24, rue Lhomond, 75 005 Paris, France*
(Received 26 April 2002; published 23 October 2002)

We report the observation of *depression* solitary surface waves on a layer of mercury when its depth is thin enough compared to the capillary length. These waves, as well as the well known *elevation* solitary waves, are studied with a new measurement technique using inductive sensors. The shape of the solitary waves, their amplitude-dependent velocity, and their damping rates by viscosity are found in good agreement with theoretical predictions.

DOI: 10.1103/PhysRevLett.89.204501 PACS numbers: 47.35.+i, 05.45.Yv, 68.03.Cd, 92.10.Hm

Since the first observation of a solitary wave on the free-surface of water by Russell [1] and its interpretation using the Korteweg–de Vries equation (KdV) [2], elevation solitary waves in shallow water have been widely studied in a quantitative way [3,4]. It has also been shown that the KdV equation generically describes a large class of solitons observed in various situations: nonlinear waves in acoustics [5], magneto-acoustic [6] or ion [7] plasma waves, elastic surface pulses [8], grey solitons in optical fibers [9], and long flexural–gravity waves in water under ice sheets [10]. It has been emphasized by Korteweg and de Vries in their early paper [2] that solitary waves may involve both a positive (*elevation*) or a negative (*depression*) localized perturbation, depending on the sign of the dispersion. However, most quantitative studies have reported the elevation solitary wave so far. In the case of waves on the surface of a fluid, only elevation solitary waves can be observed in the long wavelength limit when gravity is dominant. For shorter wavelengths, when surface tension is no longer negligible, capillary effects have a drastic influence both on extended waves (observation of ripples or parasitic waves [11]) and on localized waves such as KdV solitary waves which are predicted to become depression waves rather than elevation ones. We report here the first observation of depression solitary waves on a thin layer of mercury. By means of an accurate quantitative analysis, they are shown to have a subsonic amplitude-dependent velocity and to keep a self-similar shape although damped by viscosity.

The experimental setup consists of a 1.5 m long horizontal Plexiglas channel, 70 mm wide, filled with mercury up to a height h: $2.12 \leq h \leq 8.5$ mm. h is measured with ± 0.02 mm precision by means of a depth gauge using a micrometric linear positioner. The properties of the fluid are density, $\rho = 13.5 \times 10^3$ kg/m^3; surface tension, $\gamma = 0.484$ N/m; and dynamic viscosity, $\eta = 1.5 \times 10^{-3}$ Ns/m^2 [12]. Surface waves are generated by a sinusoidal or impulsional excitation provided by the horizontal motion of rectangular plunging Teflon wavemaker driven by an electromagnetic vibration exciter (Brüel & Kjær, type 4809). Waves are generated 10 mm inward from one end of the channel, and the local displacement of the fluid in response to this excitation is measured by two nonintrusive inductive sensors (eddy-current linear displacement gauge, Electro 4953 sensors). Both sensors, 3 mm in diameter, are suspended perpendicular to the fluid surface at rest. They are put 2.5 mm (0.5 mm) above the surface when studying elevation solitary waves (depression solitary waves). The linear sensing range of the sensors allows distance measurements from the sensor head to the fluid surface up to 2.5 mm with a 5 V/mm sensitivity. The first sensor is located 100 mm away from the wavemaker, whereas the second one is mounted on a horizontal linear positioner at a distance x from the first one, $0 < x < 1.2$ m. Although inductive sensors are widely used to get precise measurements of the position of plane metallic plates, their response in the case of a wavy liquid surface was not known. Thus, we first checked our measurements with an optical determination of the local slope of the surface: using a position sensitive detector, we recorded the deflection of a laser beam by the surface wave; the computation of the surface elevation from the optical signal was found in perfect agreement with the direct inductive measurement of the shape of the wave [13]. Although the sensitivity of the optical technique and its spatial resolution are better, the inductive method allows a direct measurement of the surface displacement and does not require signal processing. Besides simplicity, this also gives more accurate measurements of complex wave shapes because small errors may accumulate due to the numerical integration necessary to process the optical signal. Both techniques are not limited by their response time in the frequency range of surface waves. The choice of mercury was motivated by the possible use of the inductive measurement technique and also because of its kinematic viscosity which is an order of magnitude smaller than that of water, thus strongly reducing wave dissipation.

We first measure the phase velocity and determine the dispersion relation of capillary-gravity surface waves in order to check our measurement technique and to find the value of the surface tension γ. To wit, the shaker is driven sinusoidally at small amplitude at frequency f varying from 5 to 25 Hz with a 0.1 Hz step. We measure the

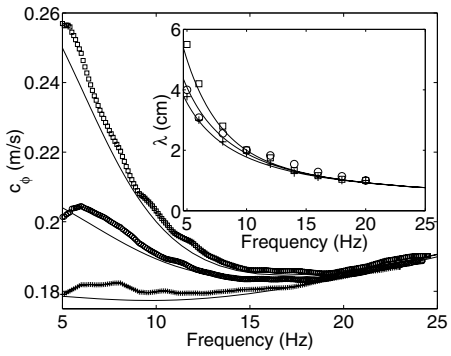

FIG. 1. Phase velocity vs f for $h = 3.3$ (+), 4.6 ($\circ$), and 8 ($\square$) mm. Solid lines represent $\omega(k)/k$ derived from Eq. (1) with $\gamma = 0.4$ N/m for $h = 3.3$ (lower curve), 4.6 (middle), and 8 (upper) mm. Inset: Wavelength versus f with additional stroboscopic measurements (same symbols as above).

relative phase difference ϕ between the signals given by the two sensors by means of a lock-in amplifier as a function of f. The phase velocity c_ϕ is then obtained from the unwrapped phase $\phi(f)$ and the distance $x = 120$ mm between the sensors: $c_\phi = 2\pi f x/\phi(f)$. It is displayed in Fig. 1 as a function of f for three different values of the height. These data are in good agreement with the dispersion relation neglecting viscosity

$$\omega = \sqrt{(gk + \tfrac{\gamma}{\rho}k^3)\tanh kh}, \tag{1}$$

between the pulsation $\omega = 2\pi f$ and the wave number k, provided that $\gamma = 0.4$ N/m, g being the acceleration of gravity. Note that this value of the surface tension is 17% lower than the tabulated one given above. This may result from the presence of contaminants at the surface which could reduce the value of the "dynamic" surface tension up to 30% with respect to the measured static value [14]. Another independent check of Eq. (1) is displayed in the inset in Fig. 1: the wavelength $\lambda = c_\phi/f$, as a function of f obtained by the previous phase method, is compared to its direct measurement using a stroboscope.

From Eq. (1), we can define the capillary length, $l_c \equiv \sqrt{\gamma/(\rho g)}$, and the Bond number, $\mathrm{Bo} \equiv (l_c/h)^2$. In the long wavelength approximation or "shallow water" limit ($k \to 0$), the linear wave velocity is $c_s = \sqrt{gh}$ and dispersion is small. When the free-surface deflection $A(x, t)$ is also small, such that nonlinear effects have the same order of magnitude as dispersive ones, it is governed to leading order by the Korteweg–de Vries equation [2]

$$A_t + \frac{3}{2}\frac{c_s}{h}AA_\xi + \frac{1}{6}c_s h^2\left(\frac{1}{3} - \mathrm{Bo}\right)A_{\xi\xi\xi} = 0, \tag{2}$$

in the comoving reference frame, $\xi \equiv x - ct$. The solitary capillary-gravity wave solution of Eq. (2) reads [2]

$$A(x, t) = A_0 \mathrm{sech}^2\left(\frac{x - ct}{L}\right), \qquad L \equiv \sqrt{\frac{4(1 - 3\mathrm{Bo})h^3}{9A_0}}, \tag{3}$$

with c the velocity of the solitary wave

$$c = c_s\left(1 + \frac{A_0}{2h}\right), \tag{4}$$

and L is the length scale of the solitary wave. Equations (3) and (4) show that there exists a continuous family of soliton solutions with parameter A_0 (the extremum amplitude of the wave). Moreover, when $0 \le \mathrm{Bo} < 1/3$, we get the previously observed elevation solitary waves ($A_0 > 0$) with supersonic speeds (Froude number $F \equiv c/c_s > 1$), whereas when $\mathrm{Bo} > 1/3$, we should find depression waves ($A_0 < 0$) with subsonic speeds ($F < 1$). In the case $\mathrm{Bo} \simeq 1/3$, an additional fifth-order dispersion term has to be taken into account

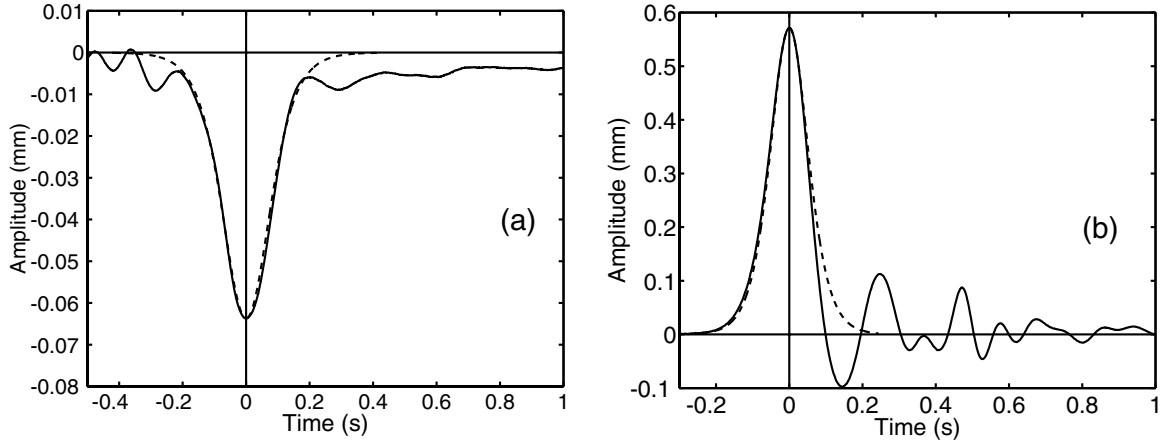

FIG. 2. (a) Free-surface profile of a *depression* solitary wave for $h = 2.12$ mm and $A_0 = 0.064$ mm, (b) *elevation* solitary wave profile for $h = 5.6$ mm and $A_0 = 0.57$ mm. Solid lines are the time recordings of the fluid surface displacement measured by the sensor located at 300 (a) and 200 (b) mm from the wavemaker. Pulse fronts are located on the left side. Dashed lines are the theoretical shapes of (a) *depression* [(b) *elevation*] KdV solitons derived from Eq. (3) with $\gamma = 0.4$ N/m, $h = 2.12$ (5.6) mm, and A_0 the minimal (maximal) amplitude of each experimental profile, leading to the following parameters of the wave: $\mathrm{Bo} = 0.67$, $L = 8.2$ mm, $\epsilon = 0.03$, $\mu = 0.07$, $\mu/\epsilon = 2.2$ ($\mathrm{Bo} = 0.1$, $L = 9.8$ mm, $\epsilon = 0.1$, $\mu = 0.32$, $\mu/\epsilon = 3.2$).

in Eq. (2), and, in this case, the solution for the full hydrodynamic problem is still a matter of theoretical debate [15,16]. Despite some trials [15,17], no conclusive observation of the depression solitary waves has been performed so far. Note that this solution of the KdV equation should not be confused with oscillatory depression waves computed in the limit of infinite depth [18] and recently observed [19].

We have performed an experimental study of solitary waves for a fluid layer height in the range $2.12 \leq h \leq 8.5$ mm; thus, $0.04 \leq \mathrm{Bo} \leq 0.67$. For mercury ($l_c = 1.74$ mm), the critical case $\mathrm{Bo} = 1/3$ corresponds to $h_c \approx 3$ mm. In order to generate solitary waves, we impulsionally drive the shaker. For $h < h_c$ ($h > h_c$), the wavemaker is horizontally drawn back (pushed forward) in order to generate a negative (positive) pulse on the fluid surface. At a given distance from the wave generator, the free-surface profile is recorded and displayed in Fig. 2(a) for a depression pulse ($h = 2.12$ mm) and in Fig. 2(b) for an elevation pulse ($h = 5.6$ mm). Both recordings are in good agreement with the profiles of depression and elevation KdV solitary wave given by Eq. (3) with $\gamma = 0.4$ N/m. Note that once A_0 is known the theoretical profile as well as the velocity of the solitary wave given by Eqs. (3) and (4) do not involve any adjustable parameter. The small oscillations observed before (after) the arrival of the pulse in Fig. 2(a) (2(b)) are identified with forerunners (or precursors) [13] and with the usual phonon radiative tail, respectively. As indicated in the caption of Fig. 2, those isolated pulses involve wave parameters that are in the range of validity required for the derivation of Eq. (2), that is, corresponding to small dispersion [$\mu \equiv (h/L)^2 \ll 1$] and small nonlinearities ($\epsilon \equiv |A|/h \ll 1$), both of the same order of magnitude.

A depression pulse for $h = 2.12$ mm is recorded at a propagation distance from the wavemaker ranging from 10 to 110 times its typical size $L \approx 10$ mm. As shown in Fig. 3, the recorded profiles are in good agreement with the KdV depression solitary wave all along the propagation. Note, however, that the first recorded pulse had not enough time to reach its asymptotic shape, and that for the last recordings, the cumulative effect of dissipation leads to a small difference from the KdV profile. In the intermediate range, the inset in Fig. 3 shows that, when expressed in the variables $-A/A_0$ and $tc|A_0|^{1/2}$, all data ($-$) lie on a single curve ($-\ -$) predicted by Eq. (3). This means that the pulse propagates with no shape deformation over a large distance with respect to its typical size and in very good agreement with the profile derived from the KdV equation.

The solitary wave velocity is measured all along its propagation by recording the time of flight between successive minima (maxima) of the amplitude A_0 for depression (elevation) pulses. The dimensionless pulse velocity, $c/\sqrt{gh}$ (Froude number F), is displayed in Fig. 4 as a function of A_0/h for various h corresponding to $0.04 \leq \mathrm{Bo} \leq 0.67$. Full (open) symbols will be used afterwards for depression (elevation) pulses. For each height corresponding to $\mathrm{Bo} > 1/3$, the velocity of the depression wave is subsonic ($F < 1$) and increases as the pulse propagates, whereas for $0 \leq \mathrm{Bo} < 1/3$, the velocity of the elevation wave is supersonic ($F > 1$) and decreases with time. All data lie on a single straight line predicted by Eq. (4), with slope 1/2 in the rescaled variables.

Finally, we study dissipative effects both on elevation and depression solitary waves. The pulse amplitude

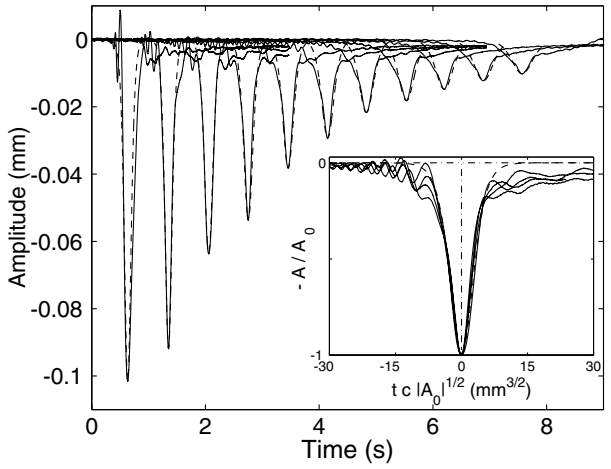

FIG. 3. Propagation of a depression solitary wave for $h = 2.12$ mm, recorded at distances from the wavemaker in the range 100 to 1100 mm with a 100 mm step. The time origin is triggered by the wavemaker. Dashed lines are the corresponding theoretical profiles of *depression* solitons derived from Eq. (3) with $\gamma = 0.4$ N/m, $h = 2.12$ mm, and A_0 the minimal amplitude of each experimental profile. The inset displays the rescaled experimental ($-$) depression solitary waves at 200, 300, 400, and 500 mm and the solution ($-\ -$) of Eq. (3).

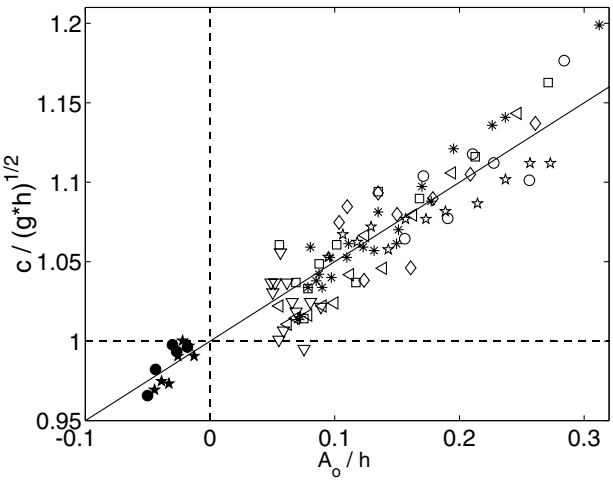

FIG. 4. Dimensionless pulse velocity $c/\sqrt{gh}$ versus A_0/h for various experimental parameters: For *depression* solitary waves, $h = 2.12$ (•) and 2.72 (★) mm. For *elevation* pulses, $h = 3.3$ (□), 3.5 (◁), 3.8 (∗), 4.5 (⋆), 4.6 (◇), 5.1 (∘), 8.5 (▽) mm. (Full line of slope 0.5).

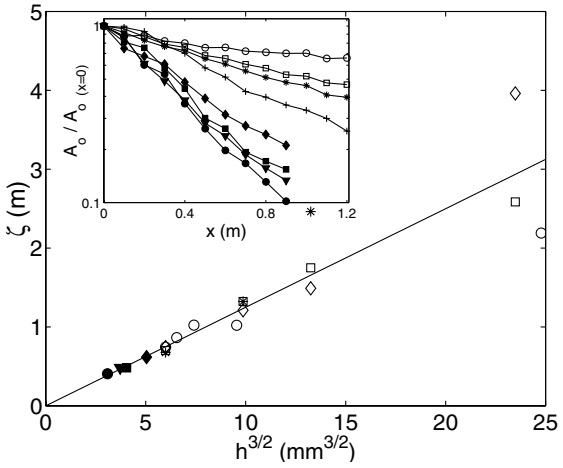

FIG. 5. Damping length versus $h^{3/2}$ for *depression* solitary waves [full symbols with $h = 2.12$ (•); 2.4 (▼); 2.54 (■); 2.94 (◆) mm for various $A_0|_{x=0}$ ($-6.2 \times 10^{-2} \leq A_0|_{x=0}/h \leq -4.3 \times 10^{-2}$)] and for *elevation* pulses [at fixed $A_0|_{x=0}/h = 0.106$ (◇); 0.285 (∗) for various $A_0|_{x=0}$ and h; at fixed $A_0|_{x=0} = 1.3$ mm (□) for various h; and at $0.1 \leq A_0|_{x=0}/h \leq 0.33$ (∘) for various $A_0|_{x=0}$ and h]. The inset displays the semi-log plot of the normalized pulse amplitude $A_0(x)/A_0|_{x=0}$ as a function of the distance x of propagation: for *depression* solitary waves (same legend as above); for *elevation* pulses with $h = 3.3$ (+); 4.6 (∗); 5.6 (□); 8.2 (∘) mm at fixed $A_0|_{x=0}/h = 0.106$. Lines join the data points.

maximum (minimum), $A_0(x)$, is displayed as a function of the propagation distance x in the inset of Fig. 5 for elevation (depression) solitary waves. We observe that $A_0(x)$ decreases exponentially with x, $A_0(x) = A_0|_{x=0} \times \exp[-x/\zeta(h)]$, where $\zeta(h)$ is the characteristic damping length. Figure 5 shows the dependence of ζ with h extracted from the slope of each linear curve in the inset. In the range, $2.12 \leq h \leq 8.5$ mm, we find that $\zeta \propto h^{3/2}$ both for depression and elevation solitary waves (see Fig. 5). This scaling can be understood as follows: for a small viscosity fluid in the shallow water limit, we have $\delta \ll h \ll L$ where δ is the size of the viscous boundary layer close to the bottom plate which gives the dominant contribution to the dissipation. From the ratio of the typical kinetic energy of the flow to the dissipated power in the boundary layer, we get a typical damping time, $\tau \propto h\delta/\nu$. This leads to the observed law, $\zeta \propto \tau c_s \propto h^{3/2}$, if we assume that δ does not depend on h. The size of the boundary layer in our experiment certainly depends on the way we generate the solitary wave, in particular, on the characteristic time scale of the initial perturbation. When this dissipation is computed from the flow generated by the KdV solitary wave alone [20], it usually underestimates the measurements done previously for elevation solitary waves on shallow water [3,21].

In conclusion, we have reported the observation of depression solitary surface waves in the shallow water limit and found that their shape and velocity are in good agreement with the ones predicted from the depression KdV solitary wave solutions. We stress that no adjustable parameter has been used to fit the pulse shape. Although the solitary waves are damped by viscous dissipation, we have shown that they keep the self-similar shape given by the continuous family of solutions of the KdV equation on a propagation length much larger than their typical scale.

We thank B. Castaing and F. Dias for discussions.

*Corresponding author.
http://www.ens-lyon.fr/~efalcon/

[1] J. S. Russell, in Proc. R. Soc. Edinburgh **11**, 319 (1844).
[2] D. J. Korteweg and G. De Vries, London, Edinburgh Dublin Philos. Mag. J. Sci. **39**, 422 (1895).
[3] J. L. Hammack and H. Segur, J. Fluid Mech. **65**, 289 (1974).
[4] A. Bettini, T. A. Minelli, and D. Pascoli, Am. J. Phys. **51**, 977 (1983).
[5] K. A. Naugol'nykh and L. A. Ostrovsky, *Nonlinear Wave Processes in Acoustics* (Cambridge University, Cambridge, 1998).
[6] T. Kakutani, H. Ono, T. Taniuti, and C.-C. Wei, J. Phys. Soc. Jpn. **24**, 1159 (1968); T. Kakutani and H. Ono, *ibid.* **26**, 1305 (1969).
[7] G. L. Lamb, *Elements of Soliton Theory* (Wiley, New York, 1980).
[8] A. M. Lomonosov, P. Hess, and A. P. Mayer, Phys. Rev. Lett. **88**, 076104 (2002).
[9] Y. S. Kivshar, Phys. Rev. A **42**, 1757 (1990).
[10] T. Takizawa, J. Geophys. Res. **93**, 5100 (1988); E. Părău and F. Dias, J. Fluid Mech. **460**, 281 (2002).
[11] A. V. Fedorov, W. K. Melville, and A. Rozenberg, Phys. Fluids **10**, 1315 (1998); J. H. Chang, R. N. Wagner, and H. C. Yuen, J. Fluid Mech. **86**, 401 (1978); G. Kuwabara, T. Hasegawa, and K. Kono, Am. J. Phys. **54**, 1002 (1986).
[12] *Handbook of Chemistry and Physics*, edited by D. R. Lide (CRC Press, New York, 1999), 80th ed.
[13] E. Falcon, C. Laroche, and S. Fauve (unpublished).
[14] D. M. Henderson and R. C. Lee, Phys. Fluids **29**, 619 (1986).
[15] T. B. Benjamin, Q. Appl. Math. **40**, 231 (1982).
[16] T. Kawahara, J. Phys. Soc. Jpn. **33**, 260 (1972); J. K. Hunter and J.-M. Vanden-Broeck, J. Fluid Mech. **134**, 205 (1983); J. A. Zufiria, J. Fluid Mech. **184**, 183 (1987); A. R. Champneys, J.-M. Vanden-Broeck, and G. J. Lord, J. Fluid Mech. **454**, 403 (2002).
[17] M. Z. Gak and E. Z. Gak, in *Nonlinear Oscillations, Waves and Vortices in Fluids International Symposium* (Center for Supercomputing Applications, St. Petersburg, 1994).
[18] M. S. Longuet-Higgins, J. Fluid Mech. **200**, 451 (1989).
[19] M. S. Longuet-Higgins and X. Zhang, Phys. Fluids **9**, 1963 (1997); X. Zhang, J. Fluid Mech. **289**, 51 (1995).
[20] G. H. Keulegan, J. Res. Natl. Bur. Stand. **40**, 487 (1948); J.W. Miles, J. Fluid Mech. **76**, 251 (1976); R. S. Johnson, *A Modern Introduction to the Mathematical Theory of Water Waves* (Cambridge University, Cambridge, 1997), pp. 365–374.
[21] P. D. Weidman and T. Maxworthy, J. Fluid Mech. **85**, 417 (1978), and references therein.